

scientific data



OPEN

DATA DESCRIPTOR

High-resolution climate projection dataset based on CMIP6 for Peru and Ecuador: BASD-CMIP6-PE

Carlos Antonio Fernandez-Palomino^{1,2}✉, Fred F. Hattermann¹, Valentina Krysanova¹, Fiorella Vega-Jácome¹, Christoph Menz¹, Stephanie Gleixner¹ & Axel Bronstert²

Here, we present BASD-CMIP6-PE, a high-resolution (1d, 10 km) climate dataset for Peru and Ecuador based on the bias-adjusted and statistically downscaled CMIP6 climate projections of 10 GCMs. This dataset includes both historical simulations (1850–2014) and future projections (2015–2100) for precipitation and minimum, mean, and maximum temperature under three Shared Socioeconomic Pathways (SSP1-2.6, SSP3-7.0, and SSP5-8.5). The BASD-CMIP6-PE climate data were generated using the trend-preserving Bias Adjustment and Statistical Downscaling (BASD) method. The BASD performance was evaluated using observational data and through hydrological modeling across Peruvian and Ecuadorian river basins in the historical period. Results demonstrated that BASD significantly reduced biases between CMIP6-GCM simulations and observational data, enhancing long-term statistical representations, including mean and extreme values, and seasonal patterns. Furthermore, the hydrological evaluation highlighted the appropriateness of adjusted GCM simulations for simulating streamflow, including mean, low, and high flows. These findings underscore the reliability of BASD-CMIP6-PE in assessing regional climate change impacts on agriculture, water resources, and hydrological extremes.

Background & Summary

Reliable hydro-climate data are essential for understanding the effects of observed and projected climate change on social and natural systems and developing effective adaptation and mitigation strategies. Several global and regional observation datasets exist at different temporal and spatial resolutions^{1–10}. At the regional scale, the Servicio Nacional de Meteorología e Hidrología del Perú (SENAMHI) has developed the Peruvian Interpolated data of Climatological and Hydrological Observations (PISCO). The PISCO dataset includes precipitation⁷, maximum and minimum temperature⁵, and reference evapotranspiration⁶ data. SENAMHI uses this dataset for drought and flood monitoring at the countrywide level of Peru. Recently a new hydrologically corrected daily precipitation dataset, called RAIN4PE (Rain for Peru and Ecuador), was developed and is available^{10,11}. RAIN4PE has proved to be superior to other existing precipitation datasets such as CHIRP², CHIRPS², ERA5⁹, MSWEP^{3,4}, and PISCO-precipitation⁷ for hydrometeorological applications and suggested to be a basis for bias adjustment of Global Climate Models (GCMs) output in Peru and Ecuador¹⁰.

GCMs have become important tools for historical climate simulation and future climate projection¹². As part of the Coupled Model Intercomparison Project (CMIP) of the World Climate Research Programme (WRCP), GCMs output has contributed to the assessment reports produced by the Intergovernmental Panel on Climate Change (IPCC)^{12–14}. Output from the latest generation of GCMs participating in the sixth phase of the CMIP (CMIP6) is now available¹⁵. CMIP6 models have a better spatial resolution (~100 km in the horizontal dimension) and physical process representation than earlier generations, as well as better simulation of recent mean climate compared to the previous CMIP phases¹⁶. Nevertheless, such a resolution is still coarse for regional and local management decisions, which need more detailed climate information. Namely, such coarse-resolution data are useless for providing a reliable base for real-world water management, particularly related to extreme hydrological conditions¹⁷. Moreover, even the latest generation of GCMs shows substantial biases^{18–20}. Therefore, it is important to bias-adjust and downscale the raw GCM outputs to produce reliable climate simulations and

¹Potsdam Institute for Climate Impact Research (PIK), Member of the Leibniz Association, PO Box 60 12 03, D-14412, Potsdam, Germany. ²Institute of Environmental Science and Geography, University of Potsdam, Potsdam, Germany.
✉e-mail: palomino@pik-potsdam.de

No.	Model	Resolution (lon. by lat.)	Member	Citation
1	CanESM5	2.8° × 2.8°	r1i1p1f1	⁵⁹
2	IPSL-CM6A-LR	2.5° × 1.3°	r1i1p1f1	⁶⁰
3	UKESM1-0-LL	1.9° × 1.3°	r1i1p1f2	⁶¹
4	CNRM-CM6-1	1.4° × 1.4°	r1i1p1f2	⁶²
5	CNRM-ESM2-1	1.4° × 1.4°	r1i1p1f2	⁶³
6	MIROC6	1.4° × 1.4°	r1i1p1f1	⁶⁴
7	GFDL-ESM4	1.3° × 1°	r1i1p1f1	⁶⁵
8	MRI-ESM2-0	1.1° × 1.1°	r1i1p1f1	⁶⁶
9	MPI-ESM1-2-HR	0.9° × 0.9°	r1i1p1f1	⁶⁷
10	EC-Earth3	0.7° × 0.7°	r1i1p1f1	⁶⁸

Table 1. List of the 10 CMIP6 models used in this study. The models are ordered from low to high spatial resolution.

Variable	Resolution	Description and source
Precipitation	Daily/0.1°	Rain for Peru and Ecuador (RAIN4PE ^{10,11})
Temperature	Daily/0.1°	Maximum and minimum temperature data for Peru ³ as provided by SENAMHI (ftp://publi_dgh2:123456@ftp.senamhi.gob.pe/)

Table 2. Climate observed data used in this study.

projections for finer-scale impact studies. To date, few studies have performed the bias adjustment and downscaling of the output of CMIP6 models, e.g., at a global scale^{21–25}, for South Asia²⁶, and for Brazil²⁷. To the best of our knowledge, there is currently no gridded dataset based on CMIP6 results bias-adjusted and downscaled for Peru and Ecuador using reliable reference data from the local observation datasets. To close this gap, we generated the new high-resolution climate dataset BASD-CMIP6-PE based on the bias-adjusted and statistically downscaled CMIP6 climate projections over Peru and Ecuador.

The BASD-CMIP6-PE dataset was generated using the trend-preserving Bias Adjustment and Statistical Downscaling (BASD) method^{28,29}. BASD effectively reduced biases between CMIP6-GCM simulations and observational data, resulting in improved representations of long-term statistical properties, including mean and extreme values, as well as seasonal patterns. BASD also demonstrated its capability to approximately preserve the projected trends and the intermodel spreads of climate variables in future climate scenarios.

A hydrological evaluation, which compared raw and adjusted GCM simulations through hydrological modeling, provided additional support for the appropriateness of adjusted GCM simulations in simulating streamflow, including mean, low, and high flows.

These advantages underscore the dataset's reliability for assessing regional climate change impacts on agriculture, water resources, and hydrological extremes, thereby supporting the development of comprehensive adaptation strategies. Notably, the BASD-CMIP6-PE dataset has already played a pivotal role in conducting the first-ever investigation into projected future changes in various components of the regional hydrological cycle and hydrological extremes across Peru, including the analysis of transboundary river catchments³⁰.

Methods

Study area. The study area covers Peru and Ecuador. The new BASD-CMIP6-PE dataset is generated for the land surface between 19°S–2°N and 82°–67°W which matches the observational data domain of the RAIN4PE and PISCO datasets. This region features complex hydroclimatic patterns arising from its diverse climate zones and the Andes Cordillera, which serves as a topographic barrier separating the cold, arid eastern Pacific from the warm, humid Amazon. These patterns result from the interplay of large-scale factors (e.g., latitudinal migration of the Atlantic Intertropical Convergence Zone, South American Monsoon Systems, marine currents, Bolivian High) and local circulation patterns (e.g., upslope and downslope moisture transport), in conjunction with the complex Andean orography^{31–34}. El Niño-Southern Oscillation (ENSO) also significantly influences interannual hydroclimatic conditions in the Andes³⁵.

Climate simulation data. Daily climate model output data for precipitation (pr) and minimum (tasmin), mean (tas), and maximum (tasmax) temperature were obtained from the CMIP6 ensemble¹⁵ for 10 GCMs (Table 1). Data were obtained for the historical simulation (1850–2014) and future projections (2015–2100), with projections run under SSP1-2.6, SSP3-7.0, and SSP5-8.5 scenarios³⁶. These ten models were also used by phase 3b of the Inter-Sectoral Impact Model Intercomparison Project (ISIMIP3b) for climate impact assessment studies^{24,25}. In terms of climate sensitivity (i.e., magnitude of the warming signal at the end of the century), the selected models are considered an appropriate choice since they approximately cover the full range of CMIP6 projections as they include models with low (GFDL-ESM4, MPI-ESM1-2-HR, MRI-ESM2-0) and high (IPSL-CM6A-LR, UKESM1-0-LL) climate sensitivity³⁷. The selected three greenhouse gas emissions scenarios span from one with mitigation policy (SSP1-2.6) to one without mitigation (SSP5-8.5) to sample future climate uncertainty from anthropogenic forcing. The SSP1-2.6 is close to the Paris Agreement goal, where global warming is limited to 2°C

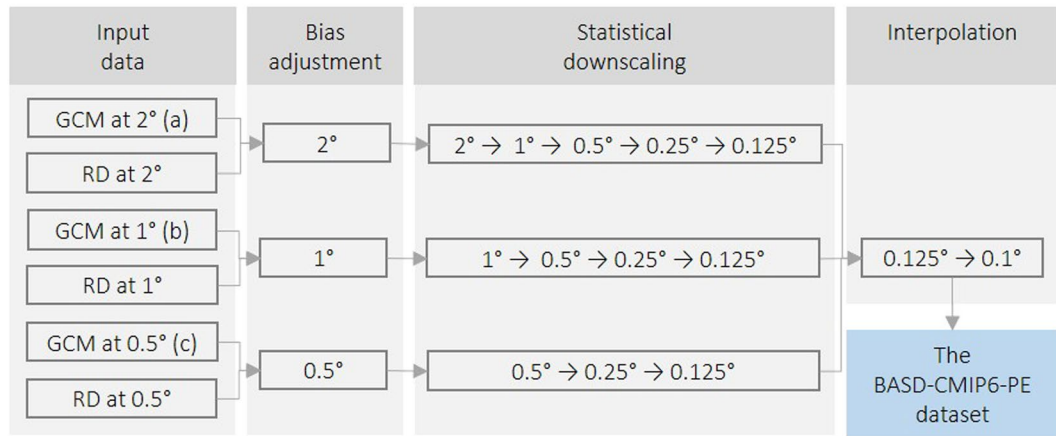


Fig. 1 Flow chart for the BASD-CMIP6-PE dataset variables (pr, tasmin, tas, tasmax) for 10 GCMs. The bias adjustment was applied at: (a) 2° for CanESM5, IPSL-CM6A-LR, and UKESM1-0-LL; (b) 1° for CNRM-CM6-1, CNRM-ESM2-1, GFDL-ESM4, MIROC6, MPI-ESM1-2-HR, and MRI-ESM2-0; and (c) 0.5° for EC-Earth3. GCM (RD) is Global Climate Model (reference) data. Note that RD are aggregated observation data.

above pre-industrial levels. The scenario is characterized by declining greenhouse gas (GHG) emissions to net zero until 2050, followed by varying levels of net negative CO₂ emissions. The SSP3-7.0 scenario is a high and the SSP5-8.5 a high-end global warming scenario with continuing high fossil fuel development throughout the 21st century and consequently strong increases in GHG emissions. For a detailed description of SSPs scenarios, refer to the Sixth Assessment Report of the IPCC¹⁴.

Climate observation. The observational reference datasets used for the evaluation, bias adjustment and statistical downscaling (BASD) of CMIP6 climate simulations are listed in Table 2. Data of precipitation (pr) were obtained from the RAIN4PE dataset^{10,11}, minimum (tasmin) and maximum (tasmax) temperature from the SENAMHI-PISCO dataset⁵, and mean temperature (tas) was estimated as the average of tasmin and tasmax. RAIN4PE precipitation data (available for 1981–2015) are generated by merging multisource precipitation data (satellite, reanalysis, and ground-based precipitation from 804 gauges) with surface elevation using the random forest method. Additionally, total precipitation was adjusted using streamflow data through the reverse hydrology method for catchments influenced by fog/cloud water input, such as páramo and montane watersheds. The PISCO temperature data (available for 1981–2016) are generated by merging information from 178 observed climate stations, satellite-derived surface temperatures, and topographic variables. The data integrate spatially gridded estimates of normal climate (estimated using weighted regression Kriging) with daily anomalies (estimated using regression splines). These observational datasets have been validated by simulating streamflow through hydrological modeling for the Peruvian and Ecuadorian catchments¹⁰.

Bias adjustment and statistical downscaling. The software used for BASD is ISIMIP3BASD v2.5²⁹ which implements the BASD method described in Lange²⁸. In ISIMIP3, this method was applied to generate bias-adjusted and downscaled CMIP6 projections, utilizing the global observational dataset W5E5 (available at a spatial resolution of 0.5°) as reference data^{24,25,38}. In our study, we adopted a different approach, employing highly reliable, region-specific, high-resolution datasets, namely PISCO-temperature and RAIN4PE precipitation, to develop BASD-CMIP6-PE. The BASD method uses 1) a trend-preserving quantile mapping approach to bias-adjust climate simulation data at their original spatial resolution using spatially aggregated climate observation data, and 2) a stochastic statistical downscaling approach to increase their spatial resolution using climate observation data, which consequently have to be available with the higher resolution. Note that bias adjustment (BA) and statistical downscaling (SD) are applied after one another and not together. Further details on the BASD method are given in Lange²⁸.

Figure 1 shows the bias adjustment and downscaling strategy to generate the BASD-CMIP6-PE dataset following the ISIMIP protocol³⁷. This dataset includes both historical simulations (1850–2014) and future projections (2015–2100) for four variables (pr, tasmin, tas, tasmax) and three future CMIP6 scenarios (SSP1-2.6, SSP3-7.0, SSP5-8.5) for 10 GCMs. To apply the ISIMIP3BASD method, the original CMIP6 output (observational data) was interpolated (aggregated) onto regular latitude-longitude grids with 0.5°, 1.0° or 2.0° resolutions using the first-order conservative remapping³⁹; Fig. 1 shows which resolution was used for each climate model. The interpolated CMIP6 data were bias-adjusted using the respective aggregated observational data and then downscaled in multiple steps. Finally, the downscaled data (0.125°) were interpolated onto 0.1° with the first-order conservative remapping method to match the spatial resolution of the observational data. This interpolation was carried out instead of downscaling due to the small resolution difference from 0.125° to 0.1°.

The training period used for bias adjustment and statistical downscaling was 1981–2014 (34 years), which was constrained by the availability of observed data and historical CMIP6 simulations. After training, we applied the bias adjustment and downscaling on the climate simulations over historical and future periods using

Criterion (reference)	Equation	Description
<i>Discharge-related performance measures</i>		
Kling-Gupta efficiency ^{69,70}	$KGE = \sqrt{(r - 1)^2 + (\beta - 1)^2 + (\gamma - 1)^2}$	r is the Pearson product-moment correlation coefficient and beta (gamma) indicates the bias (relative dispersion) between reference and simulated flows
Percent bias ⁷¹	$PBIAS = \frac{\sum_{l=1}^n (S_l - R_l)}{\sum_{l=1}^n R_l} \times 100$	n is the number of observations under evaluation
<i>Signature measures based on the flow duration curve (FDC)</i>		
Percent bias in FDC high segment volume ⁷²	$S_{high} = \frac{\sum_{h=1}^H (S_h - R_h) \times 100}{\sum_{h=1}^H R_h}$	$h = 1, 2, \dots, H$ are flow indices located within the high flow segment (0–5% flow EP)
Percent bias in FDC low segment volume ⁷²	$S_{low} = \frac{\sum_{l=1}^L (S_l - R_l) \times 100}{\sum_{l=1}^L R_l}$	$l = 1, 2, \dots, L$ are flow indices located within the low flow segment (95–100% flow EP)

Table 3. Statistical metrics and hydrological signatures. Here, R and S are the reference and simulated flow ($\text{m}^3 \text{s}^{-1}$), respectively; EP is exceedance probability; H and L are the indices of the minimum flow of the high flow and low flow segments, respectively.

contiguous 36-yr segments. This decomposition is recommended to keep a similar sample size in the training and application steps. Bias adjustment was applied using a running window with a width of 31 days and moved over the annual cycle in the step of 1 day, where results for the central day of each window constitute the overall result. This application pattern aimed to improve the annual cycle representation and reduce discontinuities at time window edges, as suggested in previous studies^{40–43}.

Evaluation approach. We conducted a comprehensive evaluation of the BASD method's performance and the reliability of the BASD-CMIP6-PE dataset for the historical period. This assessment included comparing the simulations from both unadjusted and adjusted CMIP6 models with observational data and employing hydrological modeling. Our primary focus was on evaluation of the models' capability in representing long-term statistical aspects, including mean values, extreme values, and the mean annual cycle. Moreover, we examined whether the BASD method influenced the preservation or alteration of the projected GCM trends (or changes) and the inter-model spread.

Model simulations and observations were compared using widely applied climate modeling statistics (e.g., mean error, correlation coefficient) and the Taylor diagram⁴⁴ for the overlapping time period 1981–2014. Mean error was used to show biases in GCM data, while the correlation coefficient assessed models' capability to represent the mean annual cycle of observations, a crucial aspect for hydrological modeling purposes. The Taylor diagram was used to summarize the performance of both unadjusted and adjusted CMIP6 models in simulating long-term climatological spatial fields, including mean and extreme values of precipitation and temperature across the entire study domain. According to the Taylor diagram, the closer the model points are to the reference point, the better the model performance is with relatively high correlation and low standard deviation and root-mean-square error (RMSE) values. Extreme values were determined by calculating the 95th percentile for precipitation and maximum temperature and the 5th percentile for minimum temperature. Note that simulations and reference data were conservatively interpolated to a $2^\circ \times 2^\circ$ latitude-longitude grid to facilitate the comparison.

The reliability of both raw GCM data and BASD-CMIP6-PE dataset for describing the climatology of climate variables (pr, tas, tasmax, and tasmin) was also evaluated through hydrological modeling since the response of the watershed's flow is primarily driven by the variations in precipitation and temperatures. This approach was used in recent years to evaluate gauge-corrected precipitation datasets in data-scarce regions^{10,45–47}, as well as raw and bias-adjusted GCM simulation data⁴⁸.

Hydrological simulations were performed using the Soil and Water Assessment Tool (SWAT) model⁴⁹. SWAT is one of the world's most widely used ecohydrological models^{50,51} and it has been successfully applied for ecohydrological modeling of Andean and Amazonian catchments in Peru and Ecuador^{10,52}. SWAT is a process-oriented, semi-distributed, and time-continuous river basin model applied to simulate hydrological processes as well as vegetation dynamics, nutrients, pesticides, and sediment loads within a basin^{49,53}. We used the SWAT model that was set up for the Peruvian and Ecuadorian watersheds (total of 1 638 793 km², including 2675 river segments), calibrated and validated over 72 stream gauges in our previous study¹⁰. It was forced by the observational reference climate data listed in Table 2 and was proven to represent well the water budget closure of catchments as well as discharge dynamics, including mean, low and high flows¹⁰. In this study, the SWAT model was run for 1981–2014 to derive the following streamflow series for the hydrological evaluation for a selected period (1984–2014):

- Qref, streamflow simulated by SWAT driven by the reference climate data listed in Table 2,
- Qgcm, the ensemble mean of the streamflow series simulated by SWAT employing raw GCM data (pr, tasmin, and tasmax) from 10 models, and
- Qbasd, the ensemble mean of the streamflow series simulated by SWAT using BASD-CMIP6-PE climate data (pr, tasmin, and tasmax) from 10 models.

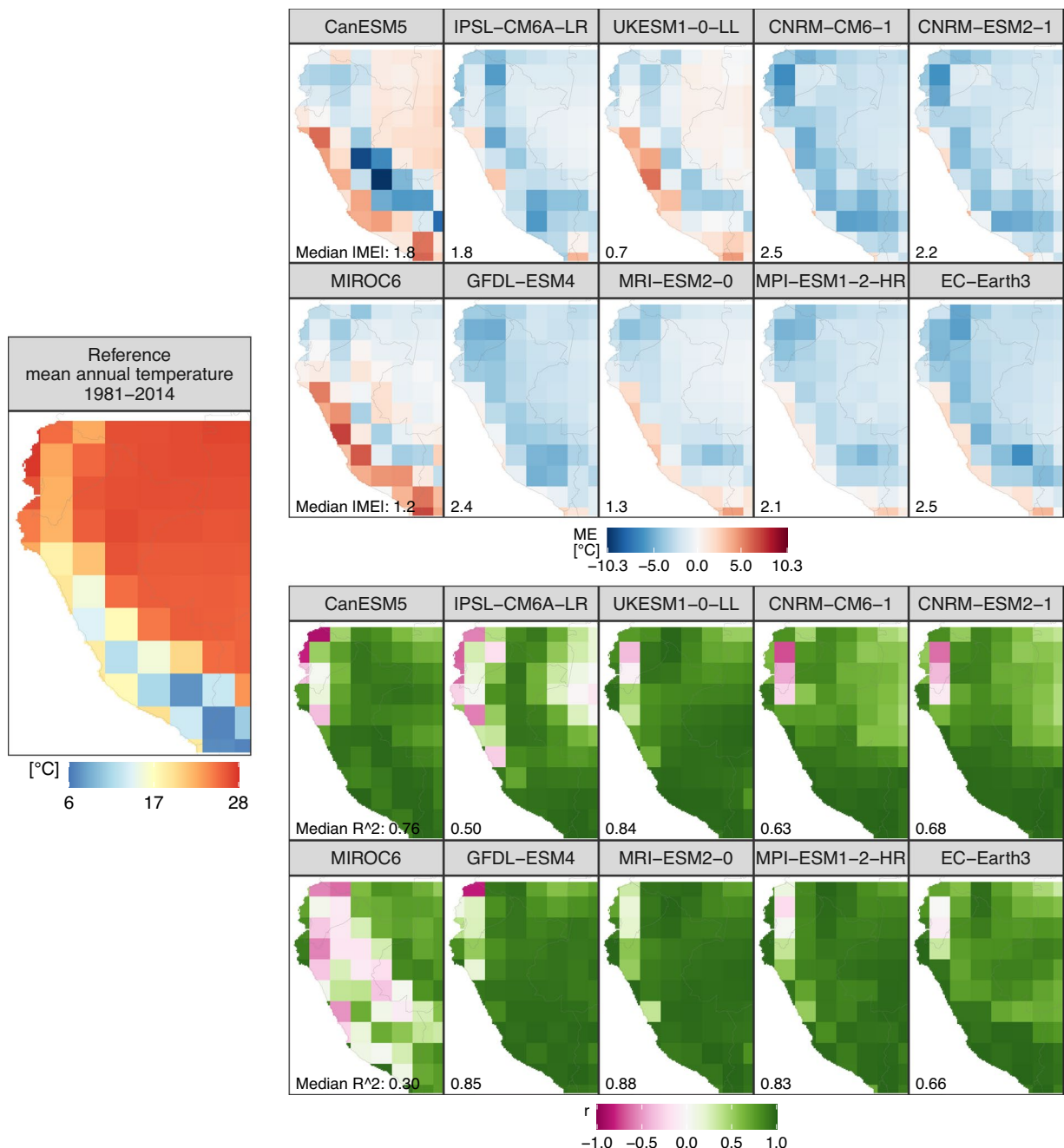


Fig. 2 Performance of the unadjusted CMIP6 models in simulating mean temperature compared with reference temperature data from PISCO-temperature for the 1981–2014 period. ME is the mean error, r is Pearson's correlation coefficient, and R^2 is the coefficient of determination. r and R^2 show the agreement between the simulated and observed mean annual temperature cycle.

The comparison between Qraw (Qbasd) and Qref reflects the reliability of the raw GCM data (BASD-CMIP6-PE dataset). For that, we used various comparison metrics based on hydrological signatures and hydrograph goodness of fit (Table 3), which were calculated using the daily values of the seasonal streamflow for the 1984–2014 period. The modified Kling-Gupta efficiency (KGE) and percent bias (PBIAS) were used for assessing model skills in representing general discharge dynamics and over or underestimation tendencies, respectively; and percent biases in flow duration curve (FDC) low segment volume (S_{low}) and FDC high segment volume (S_{high}) for low flows and high flows, respectively. In this multicriteria evaluation, all aspects of the FDC and hydrographs are assessed, which is important for assessing the reliability of climate simulation data for hydroclimatic applications, including extremes (floods and low flows). The best-fit value for PBIAS, S_{low} , and S_{high} is 0, and the best fit for KGE is 1.

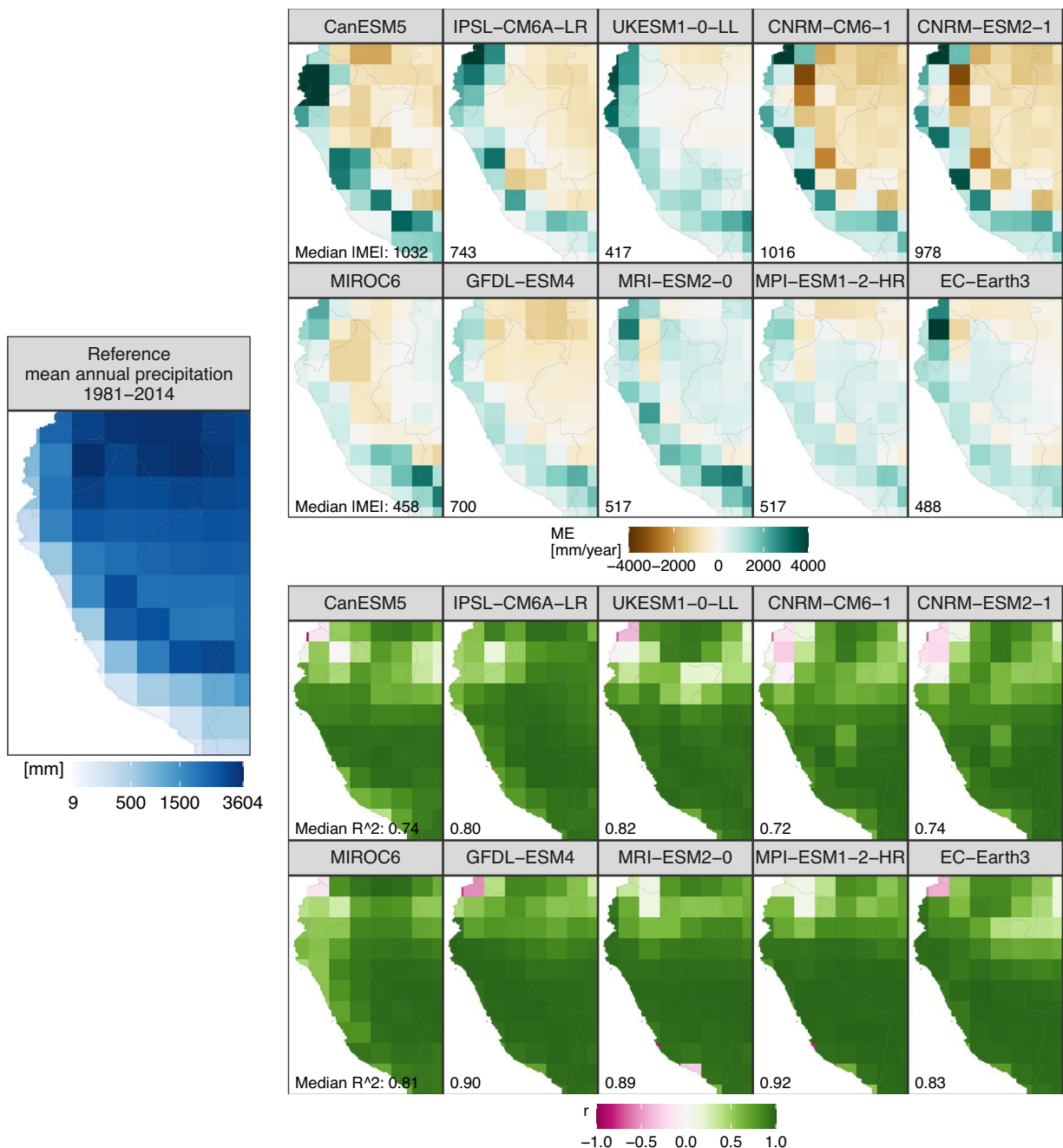


Fig. 3 Performance of the unadjusted CMIP6 models in simulating precipitation compared with reference precipitation data from RAIN4PE for the 1981–2014 period. ME is the mean error, r is Pearson's correlation coefficient, and R^2 is the coefficient of determination. r and R^2 show the agreement between the simulated and observed mean annual precipitation cycle.

Data Records

The BASD-CMIP6-PE dataset⁵⁴ is freely available under the CC BY 4.0 license at <https://doi.org/10.5880/pik.2023.001>. BASD-CMIP6-PE provides bias-adjusted and statistically downscaled CMIP6 climate projections, encompassing four meteorological variables: precipitation (pr), minimum temperature (tasmin), mean temperature (tas), and maximum temperature (tasmax). These data cover both the historical period (1850–2014) and future projections (2015–2100) under three different CMIP6 experiments (SSP1-2.6, SSP3-7.0, and SSP5-8.5) for 10 CMIP6-GCMs. Precipitation data is reported in millimeters (mm), while temperature data is presented in degrees Celsius (°C). The total size of the dataset is 374 GB.

The BASD-CMIP6-PE dataset is organized within a “daily” folder, denoting its availability at a daily temporal resolution. Within this directory, four subfolders are present: “historical” containing historical data, “ssp126” for SSP1-2.6, “ssp370” for SSP3-7.0, and “ssp585” for SSP5-8.5. Each of these subfolders further includes ten distinct folders, corresponding to different GCMs: CanESM5, IPSL-CM6A-LR, UKESM1-0-LL, CNRM-CM6-1,

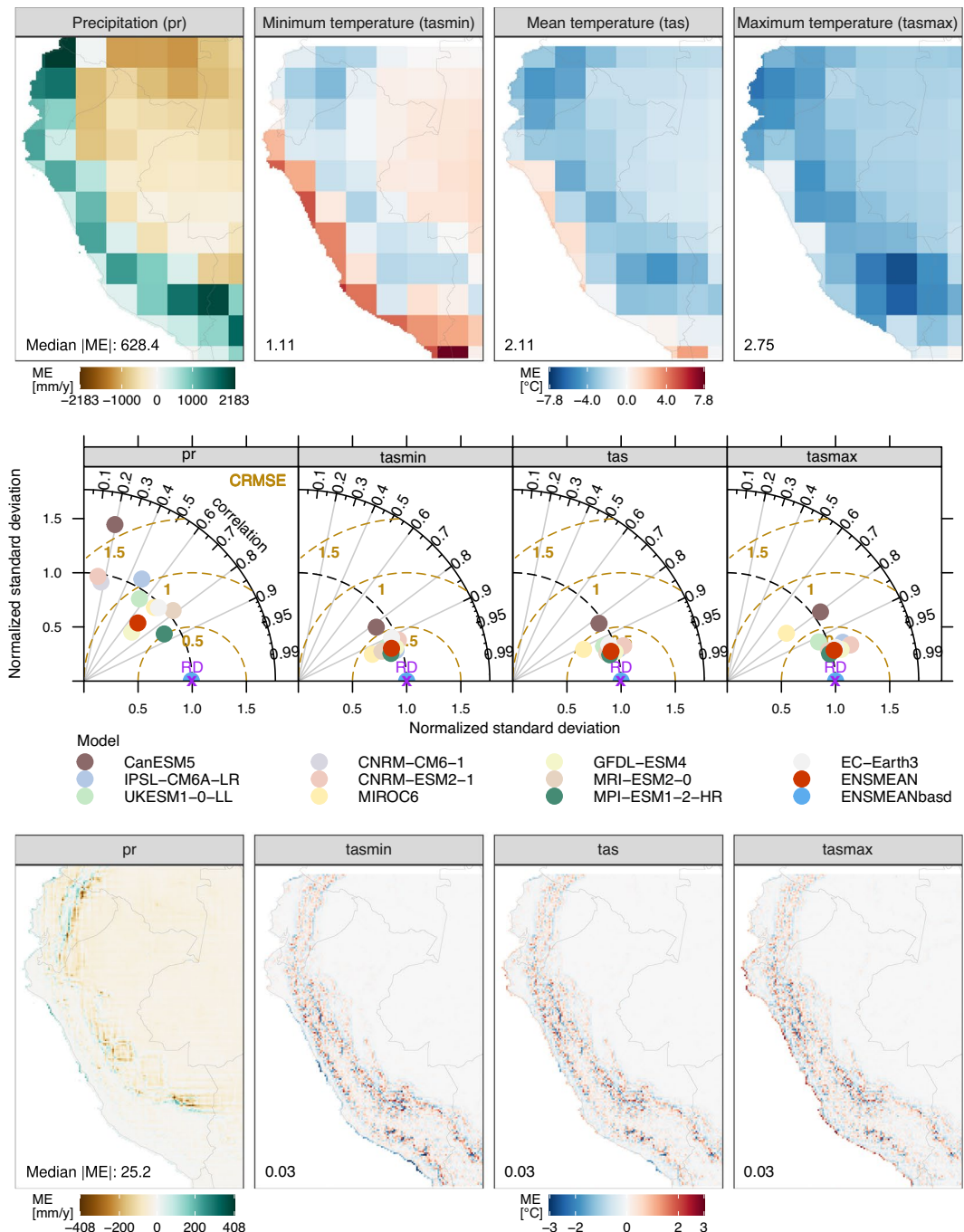


Fig. 4 Mean Errors [ME] in (Top) unadjusted [ENSMEAN] and (Bottom) adjusted [ENSMEANbasd] CMIP6 multimodel ensemble means, and (Middle) Taylor diagrams, both comparing simulated and reference climate means for 1981–2014. Adjusted models were excluded from the Taylor diagrams as they closely match ENSMEANbasd and the reference data. The bottom panel displays ME in ENSMEANbasd, computed by comparing BASD-CMIP6-PE and observational data at a 0.1° spatial resolution.

CNRM-ESM2-1, MIROC6, GFDL-ESM4, MRI-ESM2-0, MPI-ESM1-2-HR, and EC-Earth3. These folders store the data in the NetCDF format arranged by model, model member, experiment, variable, temporal resolution, and subset period, resulting in file names like “canesm5_r1i1p1f1_ssp126_pr_daily_2015_2020.nc”.

Technical Validation

Comparison of unadjusted and adjusted CMIP6 models for the historical period. *Mean climate and seasonality.* Outputs of the atmospheric variables (pr, tasmin, tas, and tasmax) obtained from CMIP6-GCMs exhibit biases (Figs. 2–4) and limitations in capturing the mean annual cycle (Figs. 2, 3). Figure 4 (top panel) shows that CMIP6 models are generally biased cold (warm) for tas and tasmax (tasmin) over the Andes

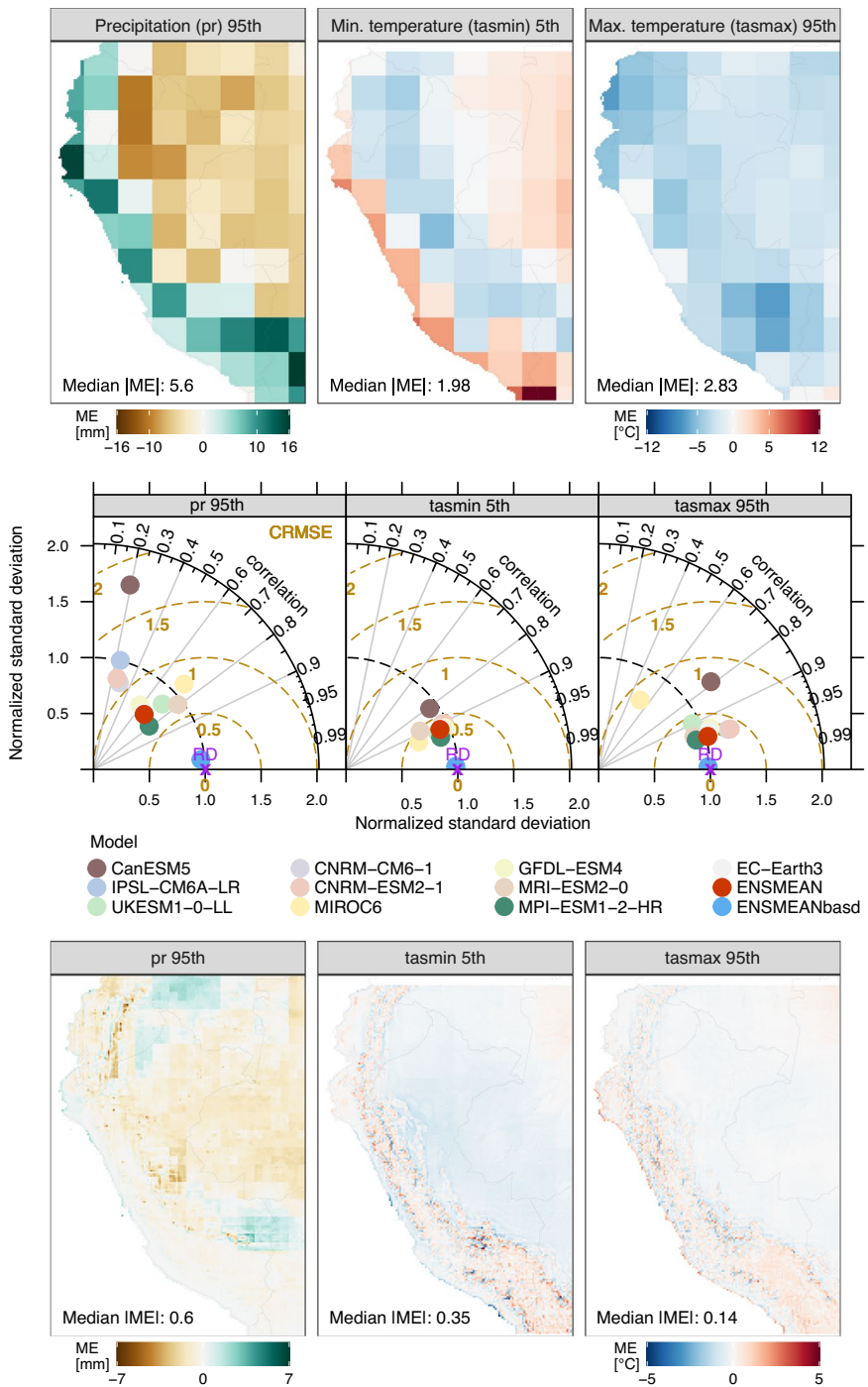


Fig. 5 Mean Errors [ME] in (Top) unadjusted [ENSMEAN] and (Bottom) adjusted [ENSMEANbasd] CMIP6 multimodel ensemble means, and (Middle) Taylor diagrams, both comparing simulated and reference climate extremes for 1981–2014. Adjusted models were excluded from the Taylor diagrams as they closely match ENSMEANbasd and the reference data. The bottom panel displays ME in ENSMEANbasd, computed by comparing BASD-CMIP6-PE and observational data at a 0.1° spatial resolution.

(Peruvian coastal areas) and tend to overestimate (underestimate) pr over the Andes (Amazon lowlands). Models simulate better the annual cycle of precipitation (Fig. 3) than temperature (Fig. 2). However, models cannot capture the annual cycle of pr over Ecuador and northwest Amazon (Fig. 3). This is critical as unadjusted data from models are useless, for example, for evaluating the hydrological impact of Peruvian and Ecuadorian catchments under climate change. The Taylor diagrams (Fig. 4, middle panel) show that the GCMs simulate better the spatial patterns of temperature (tasmin, tas, and tasmax) than the precipitation patterns. The models simulate a realistic spatial variability (standard deviation similar to that of reference) of precipitation, but the correlation between the spatial patterns is weak for most models (between 0.13 and 0.86). In the same Fig. 4 (middle panel),

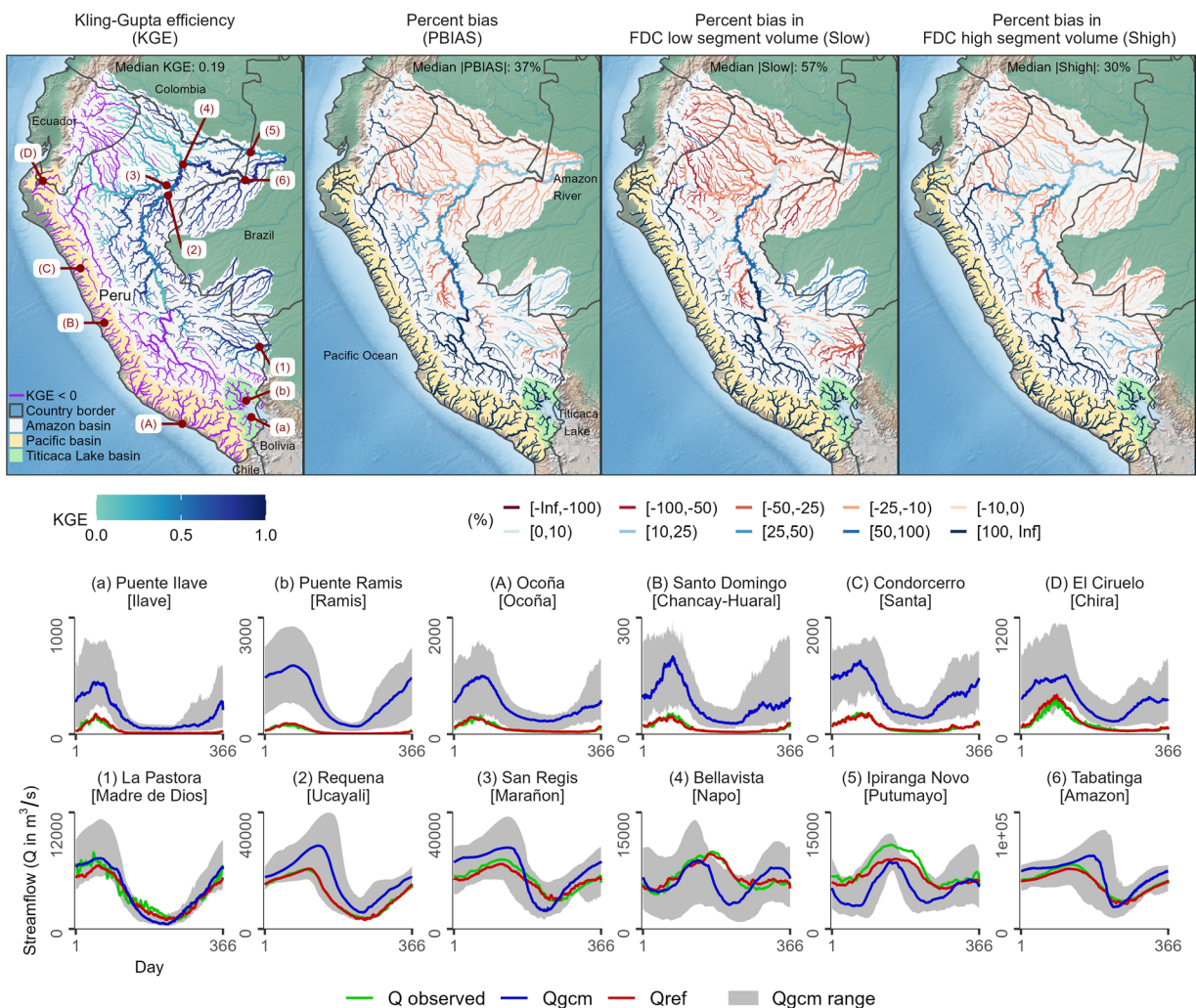


Fig. 6 Comparison of simulated streamflow dynamics, including extreme events of both low flows (S_{low}) and high flows (S_{high}), from raw GCM simulations (Q_{gcm}) and reference climate-based simulated streamflow (Q_{ref}). (top) Statistical metrics and hydrological signatures and (bottom) daily values of climatological seasonal streamflow (Q) in the period 1984–2014 for representative river catchments draining into the Titicaca Lake (a,b), the Pacific Ocean (A:D), and the Amazon River (1:6). Note that observed seasonal streamflow was computed only using the days with available streamflow data.

the Taylor diagram component values (correlation, standard deviation, and RMSE) indicate that the MPI-ESM1-2-HR (CanESM5) model has the best (worst) performance in simulating all atmospheric variables analyzed in this study. This distinction is emphasized by the general proximity of MPI-ESM1-2-HR points to the reference point, while CanESM5 points are situated farther away.

Overall, our results reveal that CMIP6 simulations (pr, tas, tasmin, and tasmax) are biased when compared to reference datasets over Peru and Ecuador, with larger biases over the Andes (Figs. 2–4). Such CMIP6 biases were also reported in previous studies^{18,55–57}. The precipitation overestimation is likely related to the too-pronounced double ITCZ in the models, a complex error in models produced by anomalous warming over the southern tropical Pacific in association with a misrepresentation of ocean-atmosphere couplings^{57,58}. Our results also reveal the limitation of CMIP6 models to reproducing the annual cycle of temperature and precipitation (Figs. 2, 3). CMIP6 models simulate the annual precipitation cycle better over regions with the strongest rainfall seasonality, such as the Peruvian Andes and lowlands, and poorly over equatorial regions, such as Ecuador and the northwest Amazon (Fig. 3). Poor representation of annual precipitation cycle by CMIP6 models was also reported over Colombia¹⁸ and Northern Amazon^{19,20}. Our results show significant limitations of CMIP6 models in reproducing regional climate features over equatorial regions and terrains with complex topography, such as the Andes. Further improvements of these models are necessary to permit their usage in impact studies.

To exclude the aforementioned limitations in climate model outputs, we applied the BASD method in order to adjust biases, increase spatial resolution, and improve representation of the annual cycle of atmospheric variables. The comparison of the ensemble mean of unadjusted (ENSMEAN) and adjusted (ENSMEAN_{basd}) outputs of 10 GCMs shows that the BASD method largely reduced the biases in the GCM data for all climate variables

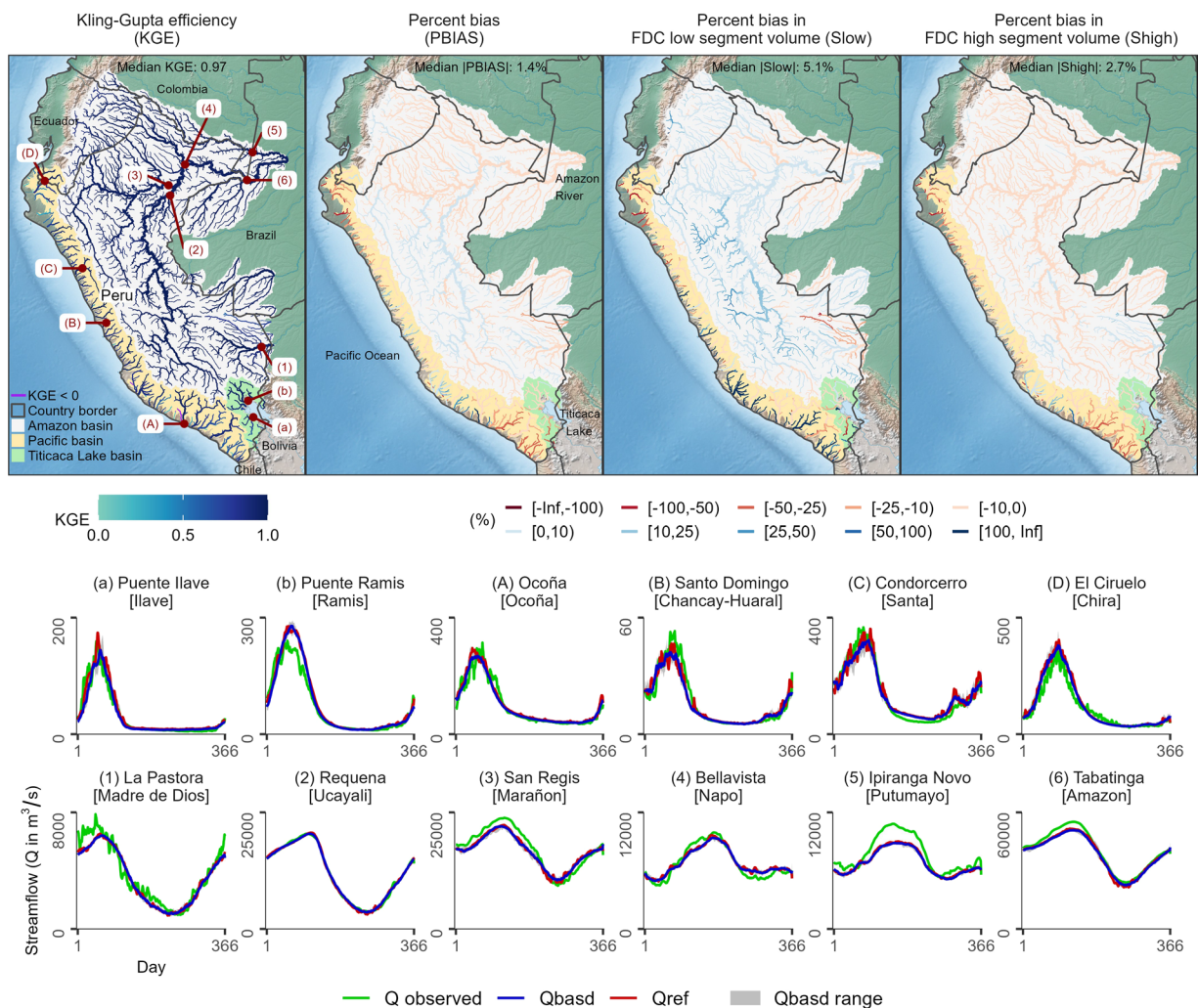


Fig. 7 Comparison of simulated streamflow dynamics, including extreme events of both low flows (S_{low}) and high flows (S_{high}), from adjusted GCM simulations (Q_{basd}) and reference climate-based simulated streamflow (Q_{ref}). (top) Statistical metrics and hydrological signatures and (bottom) daily values of climatological seasonal streamflow (Q) in the period 1984–2014 for representative river catchments draining into the Titicaca Lake (a,b), the Pacific Ocean (A:D), and the Amazon River (1:6). Note that observed seasonal streamflow was computed only using the days with available streamflow data.

(pr, tasmin, tas, and tasmax) as shown in Fig. 4 (middle panel). However, there are remaining biases after the application of BASD at the spatial resolution of the reference datasets at 0.1° (Fig. 4, bottom panel). Small biases of precipitation remain over precipitation hotspots and small temperature biases (tasmin, tas, and tasmax) along the Andes. These results indicate that the application of BASD to the output of CMIP6 models is challenging in terrains with complex topography, such as the Andes. Despite some remaining biases, the purpose of the method - to create a dataset suitable for hydrological modeling - has been achieved, as the following hydrological section demonstrates.

Extreme values. The assessment of the models' performance in simulating precipitation and temperature extremes, both before and after applying BASD, is shown in Fig. 5. In this figure, Taylor diagrams compare the degree of similarity in spatial patterns of extremes, considering their correlation, RMSE, and standard deviation.

Results show that CMIP6 models, particularly CanESM5, exhibit poor performance in simulating extreme values, as indicated by Taylor diagrams (Fig. 5, middle panel). Figure 5 (top panel) shows notable biases in the unadjusted multimodel ensemble (ENSMEAN), with distinct spatial patterns. ENSMEAN tends to overestimate extreme precipitation along the Andes while underestimating it over the Amazon lowland regions. Moreover, it exhibits a warm bias in extreme minimum temperatures in coastal areas and the Brazilian lowlands, while concurrently revealing a cold bias in the transitional zone between the Andes and the Amazon. A cold bias is also observed in extreme maximum temperatures across the entire study area.

These biases are substantially reduced by the adjusted multimodel ensemble (ENSMEANbasd) for all extreme climatic variables assessed herein, as demonstrated by Taylor diagrams (Fig. 5, middle panel) and the

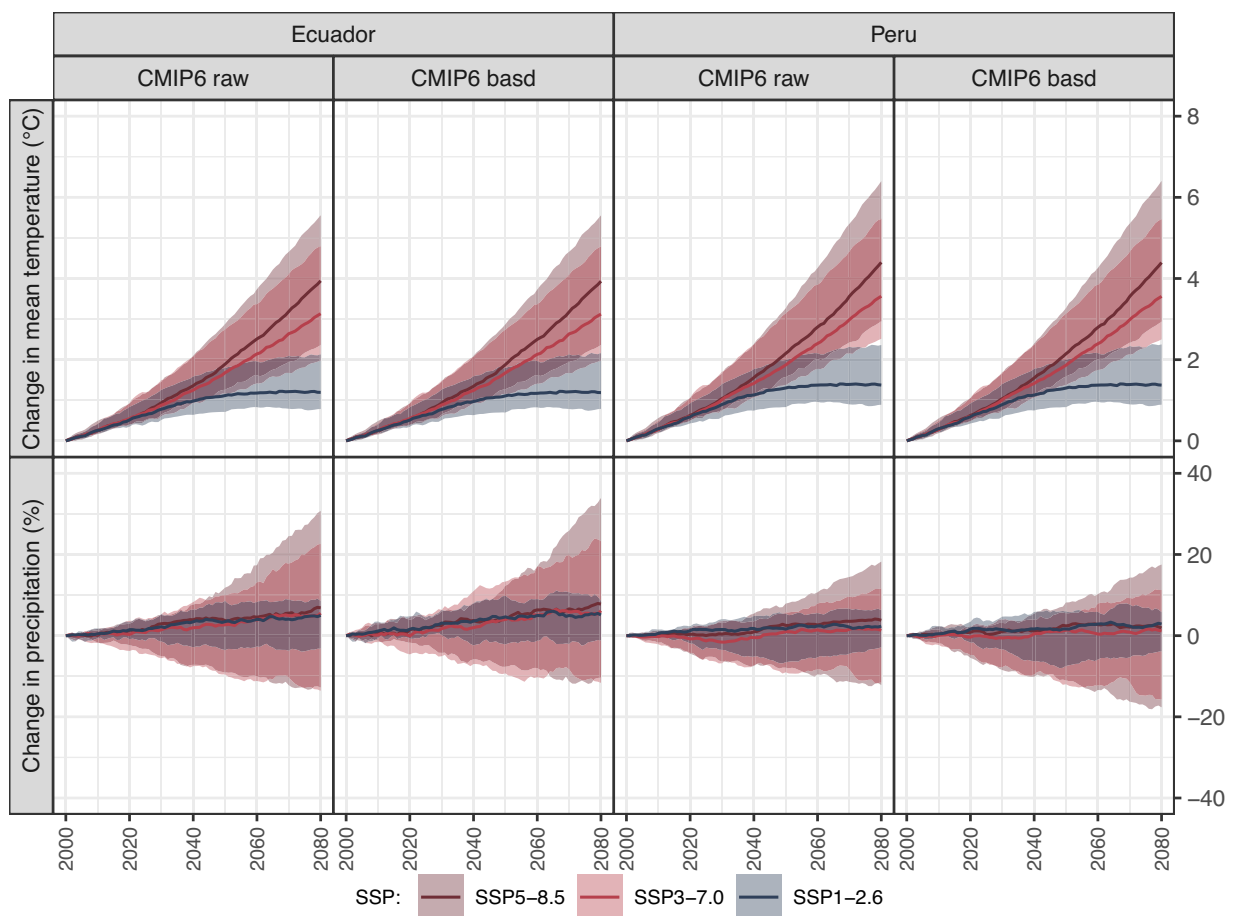


Fig. 8 Comparison of projected multimodel median changes and spreads in precipitation and mean temperature for Ecuador and Peru using raw (CMIP6 raw) and adjusted (CMIP6 basd) GCM simulations.

adjusted CMIP6 multimodel mean errors (Fig. 5, bottom panel). The results clearly show that the BASD method improves the variability and extremes of precipitation and temperature, thereby establishing the reliability of the BASD-CMIP6-PE dataset for studying the impacts of climate change on extreme events.

Hydrological evaluation of unadjusted and adjusted CMIP6 models for the historical period. In Fig. 6 (or Fig. 7), a comparison is presented between the long-term mean annual streamflow cycle at a daily resolution derived from Qgcm (or Qbasd) and that derived from Qref. The comparison is made through statistical metrics (KGE and PBIAS) and hydrological signatures (S_{low} and S_{high}). These figures also show climatological seasonal streamflow plots for representative river catchments draining into the Titicaca Lake, the Pacific Ocean, and the Amazon River.

In Fig. 6, the comparison metrics (with median values of $KGE = 0.19$, $|PBIAS| = 37\%$, $|S_{low}| = 57\%$, and $|S_{high}| = 30\%$) alongside seasonal streamflow plots reveal significant discrepancies in the mean annual streamflow cycle between Qgcm and Qref. These disparities indicate that hydrological model simulations using raw GCM data tend to overestimate mean, low, and high flows along the Andean rivers while underestimating them over Amazonian lowland tributaries, especially in the northern Peruvian Amazon and Ecuadorian Amazon. Additionally, these simulations underrepresent seasonal streamflow in these regions, as evidenced by the seasonal plots for the Marañón, Napo, and Putumayo rivers. These issues underscore how biases and regional seasonal underrepresentation in GCM simulations impact the accurate representation of hydrological processes, rendering them unsuitable for hydrological impact assessments.

In Fig. 7, median $KGE = 0.97$ and median $|PBIAS| = 1.4\%$ demonstrate good agreement between Qbasd and Qref. This agreement is further supported by long-term mean seasonal streamflow plots for representative rivers across the three drainage systems. Low $KGE (< 0.5)$ and large negative PBIAS values ($< -25\%$) indicate relatively poor BASD performance over northern and southern Peruvian arid coastal areas in the Pacific drainage system. It is worth noting that these areas have mean annual precipitation of less than 15 mm and are not relevant for runoff processes. Median $|S_{low}| = 5.1\%$ and median $|S_{high}| = 2.7\%$ also indicate that overall low and high flows are well represented, suggesting that the BASD method is able to represent also precipitation extremes to some extent. However, there is a tendency to overestimate low flows over river segments in the eastern slopes of the Peruvian Andes, especially over mountainous catchments.

Overall, the hydrological comparisons reveal much better agreement between Qbasd and Qref (median KGE = 0.97) compared to Qgcm and Qref (median KGE = 0.19) across different hydroclimate regimes in Peru and Ecuador. This indicates that the BASD method is effective, and the BASD-CMIP6-PE dataset is reliable for hydroclimatic applications, including extremes such as floods and droughts. However, it is important to keep in mind that the hydrological evaluation was performed for the period where the BASD method was trained, and our evaluation results could be overconfident. Nevertheless, we believe that our hydrological evaluation is still plausible in the study area featured by data scarcity and lack of long-term time series.

Projected changes and inter-model spread. The assessment of the BASD method's impact on preserving or altering the projected GCM trends and the inter-model spread is presented in Fig. 8. This figure presents the projected multimodel median changes and spreads in precipitation and mean temperature for both Ecuador and Peru, using both unadjusted and adjusted CMIP6 data.

Results show that temperature trends and spreads show a significant degree of similarity between the two datasets in each country, highlighting the effectiveness of the BASD method in preserving future temperature trends. For Ecuador, the projected changes in mean temperature for the end of the century (2065–2095) relative to the reference period of 1985–2015, based on both raw and adjusted multimodel median data, are 1.2 °C (SSP1-2.6), 3.1 °C (SSP3-7.0), and 3.9 °C (SSP5-8.5). For Peru, these values are 1.4 °C (SSP1-2.6), 3.6 °C (SSP3-7.0), and 4.4 °C (SSP5-8.5).

However, the projected multimodel median changes and spreads for precipitation undergo minor modifications. The differences in projected changes for the end of the century, based on raw and adjusted CMIP6 data, are less than 2% across all SSPs for both Ecuador and Peru. These small differences suggest that the BASD method alters precipitation patterns without adversely affecting the ensemble median. Projected multimodel median changes in precipitation can range up to 8% in Ecuador and 3% in Peru, with variations within these countries.

It is noteworthy that intermodel spread increases towards the distant future, with low uncertainty under SSP1-2.6 and high uncertainty under SSP5-8.5.

In summary, our analysis indicates that the BASD method effectively preserves projected temperature trends while making only minor adjustments to precipitation patterns. This underscores the reliability of the BASD-CMIP6-PE dataset for evaluating regional and local hydrological impacts of climate change.

Code availability

The software used for bias adjustment and statistical downscaling is ISIMIP3BASD v2.5²⁹.

Received: 3 February 2023; Accepted: 15 December 2023;

Published online: 05 January 2024

References

1. Funk, C. *et al.* A global satellite-assisted precipitation climatology. *Earth Syst. Sci. Data* **7**, 275–287 (2015).
2. Funk, C. *et al.* The climate hazards infrared precipitation with stations - A new environmental record for monitoring extremes. *Sci. Data* **2**, 1–21 (2015).
3. Beck, H. E. *et al.* MSWEP: 3-hourly 0.25° global gridded precipitation (1979–2015) by merging gauge, satellite, and reanalysis data. *Hydroclim. Earth Syst. Sci.* **21**, 589–615 (2017).
4. Beck, H. E. *et al.* MSWEP V2 Global 3-Hourly 0.1° Precipitation: Methodology and Quantitative Assessment. *Bull. Am. Meteorol. Soc.* **100**, 473–500 (2019).
5. Huerta, A., Aybar, C. & Lavado-Casimiro, W. *PISCO temperatura v.1.1. SENAMHI - DHI-2018, Lima-Perú*. http://iridl.ldeo.columbia.edu/documentation/pisco/PISCOT_report.pdf (2018).
6. Huerta, A. *et al.* PISCOeo_pm, a reference evapotranspiration gridded database based on FAO Penman-Monteith in Peru. *Sci. Data* **2022** *9*, 1–18 (2022).
7. Aybar, C. *et al.* Construction of a high-resolution gridded rainfall dataset for Peru from 1981 to the present day. *Hydroclim. Sci. J.* **65**, 770–785 (2020).
8. Harris, I., Osborn, T. J., Jones, P. & Lister, D. Version 4 of the CRU TS monthly high-resolution gridded multivariate climate dataset. *Sci. Data* **7**, 1–18 (2020).
9. Hersbach, H. *et al.* The ERA5 Global Reanalysis. *Q. J. R. Meteorol. Soc.* **146**, 1999–2049 (2020).
10. Fernandez-Palomino, C. A. *et al.* A novel high-resolution gridded precipitation dataset for Peruvian and Ecuadorian watersheds – development and hydrological evaluation. *J. Hydrometeorol.* **1**, (2021).
11. Fernandez-Palomino, C. A. *et al.* Rain for Peru and Ecuador (RAIN4PE). V. 1.0. GFZ Data Serv. <https://doi.org/10.5880/piK.2020.010> (2021).
12. IPCC. *Climate Change 2007: The Physical Science Basis. Contribution of Working Group I to the Fourth Assessment Report of the Intergovernmental Panel on Climate Change.* (Cambridge University Press, 2007).
13. IPCC. *Climate Change 2013: The Physical Science Basis. Contribution of Working Group I to the Fifth Assessment Report of the Intergovernmental Panel on Climate Change.* (Cambridge University Press, 2013).
14. IPCC. *Climate Change 2021: The Physical Science Basis. Contribution of Working Group I to the Sixth Assessment Report of the Intergovernmental Panel on Climate Change.* <https://doi.org/10.1017/9781009157896> (Cambridge University Press, 2021).
15. Eyring, V. *et al.* Overview of the Coupled Model Intercomparison Project Phase 6 (CMIP6) experimental design and organization. *Geosci. Model Dev.* **9**, 1937–1958 (2016).
16. Eyring, V. *et al.* Reflections and projections on a decade of climate science. *Nat. Clim. Chang.* **2021** *11*, 279–285 (2021).
17. Bronstert, A., Kolokotronis, V., Schwandt, D. & Straub, H. Comparison and evaluation of regional climate scenarios for hydrological impact analysis: General scheme and application example. *Int. J. Climatol.* **27**, 1579–1594 (2007).
18. Arias, P. A. *et al.* Colombian climatology in CMIP5/CMIP6 models: Persistent biases and improvements. *Rev. Fac. Ing. Univ. Antioquia* **75–96**, <https://doi.org/10.17533/UDEA.REDIN.20210525> (2021).
19. Firpo, M. Á. F. *et al.* Assessment of CMIP6 models' performance in simulating present-day climate in Brazil. *Front. Clim.* **0**, 170 (2022).
20. Monteverde, C., De Sales, F. & Jones, C. Evaluation of the CMIP6 Performance in Simulating Precipitation in the Amazon River Basin. *Climate* **10**, 122 (2022).

21. Xu, Z., Han, Y., Tam, C. Y., Yang, Z. L. & Fu, C. Bias-corrected CMIP6 global dataset for dynamical downscaling of the historical and future climate (1979–2100). *Sci. Data* 2021 **8**, 1–11 (2021).
22. Thrasher, B. *et al.* NASA Global Daily Downscaled Projections, CMIP6. *Sci. Data* 2022 **9**, 1–6 (2022).
23. Noël, T., Loukos, H., Defrance, D., Vrac, M. & Levavasseur, G. Extending the global high-resolution downscaled projections dataset to include CMIP6 projections at increased resolution coherent with the ERA5-Land reanalysis. *Data Br.* **45**, 108669 (2022).
24. Lange, S. & Büchner, M. ISIMIP3b bias-adjusted atmospheric climate input data. *ISIMIP Repos.* <https://doi.org/10.48364/ISIMIP.842396.1> (2021).
25. Lange, S. & Büchner, M. Secondary ISIMIP3b bias-adjusted atmospheric climate input data. *ISIMIP Repos.* <https://doi.org/10.48364/ISIMIP.581124> (2022).
26. Mishra, V., Bhatia, U. & Tiwari, A. D. Bias-corrected climate projections for South Asia from Coupled Model Intercomparison Project-6. *Sci. Data* **7**, 1–13 (2020).
27. Ballarin, A. S. *et al.* CLIMBra - Climate Change Dataset for Brazil. *Sci. Data* **10**, 1–16 (2023).
28. Lange, S. Trend-preserving bias adjustment and statistical downscaling with ISIMIP3BASD (v1.0). *Geosci. Model Dev.* **12**, 3055–3070 (2019).
29. Lange, S. ISIMIP3BASD (2.5.0). *Zenodo* <https://doi.org/10.5281/ZENODO.4686991> (2021).
30. Fernandez-Palomino, C. A. *et al.* Pan-Peruvian Simulation of Present and Projected Future Hydrological Conditions Using Novel Data Products and CMIP6 Climate Projections. *SSRN* <https://doi.org/10.2139/SSRN.4602668> (2023).
31. Laraque, A., Ronchail, J., Cochonneau, G., Pombosa, R. & Guyot, J. L. Heterogeneous distribution of rainfall and discharge regimes in the Ecuadorian Amazon basin. *J. Hydrometeorol.* **8**, 1364–1381 (2007).
32. Tobar, V. & Wyseure, G. Seasonal rainfall patterns classification, relationship to ENSO and rainfall trends in Ecuador. *Int. J. Climatol.* **38**, 1808–1819 (2018).
33. Segura, H. *et al.* New insights into the rainfall variability in the tropical Andes on seasonal and interannual time scales. *Clim. Dyn.* **53**, 405–426 (2019).
34. Espinoza, J. C. *et al.* Hydroclimate of the Andes Part I: Main Climatic Features. *Front. Earth Sci.* **8**, 64 (2020).
35. Poveda, G. *et al.* High Impact Weather Events in the Andes. *Front. Earth Sci.* **8**, (2020).
36. Riahi, K. *et al.* The Shared Socioeconomic Pathways and their energy, land use, and greenhouse gas emissions implications: An overview. *Glob. Environ. Chang.* **42**, 153–168 (2017).
37. Lange, S. *ISIMIP3b bias adjustment fact sheet*. https://www.isimip.org/documents/413/ISIMIP3b_bias_adjustment_fact_sheet_Gnsz7CO.pdf (2021).
38. Lange, S. *et al.* WFDE5 over land merged with ERA5 over the ocean (W5E5 v2.0). *ISIMIP Repos.* <https://doi.org/10.48364/ISIMIP.342217> (2021).
39. Jones, P. W. First- and Second-Order Conservative Remapping Schemes for Grids in Spherical Coordinates. *Mon. Weather Rev.* **127**, 2204–2210 (1999).
40. Themelis, M. J., Gobiet, A. & Heinrich, G. Empirical-statistical downscaling and error correction of regional climate models and its impact on the climate change signal. *Clim. Change* **112**, 449–468 (2012).
41. Thrasher, B., Maurer, E. P., McKellar, C. & Duffy, P. B. Technical Note: Bias correcting climate model simulated daily temperature extremes with quantile mapping. *Hydrol. Earth Syst. Sci.* **16**, 3309–3314 (2012).
42. Gennaretti, F., Sangelantoni, L. & Grenier, P. Toward daily climate scenarios for Canadian Arctic coastal zones with more realistic temperature–precipitation interdependence. *J. Geophys. Res. Atmos.* **120**, 11862–11877 (2015).
43. Grenier, P. Two Types of Physical Inconsistency to Avoid with Univariate Quantile Mapping: A Case Study over North America Concerning Relative Humidity and Its Parent Variables. *J. Appl. Meteorol. Climatol.* **57**, 347–364 (2018).
44. Taylor, K. E. Summarizing multiple aspects of model performance in a single diagram. *J. Geophys. Res.* **106**, 7183 (2001).
45. Beck, H. E. *et al.* Global-scale evaluation of 22 precipitation datasets using gauge observations and hydrological modeling, in *Advances in Global Change Research* (eds. Levizzani, V. *et al.*) **vol. 69** 625–653 (Springer International Publishing, 2020).
46. Brocca, L. *et al.* River flow prediction in data scarce regions: soil moisture integrated satellite rainfall products outperform rain gauge observations in West Africa. *Sci. Rep.* **10**, 12517 (2020).
47. Satgé, F. *et al.* Reliability of SM2RAIN precipitation datasets in comparison to gauge observations and hydrological modelling over arid regions. *Int. J. Climatol.* **41**, E517–E536 (2020).
48. Hakala, K., Addor, N. & Seibert, J. Hydrological Modeling to Evaluate Climate Model Simulations and Their Bias Correction. *J. Hydrometeorol.* **19**, 1321–1337 (2018).
49. Arnold, J. G., Srinivasan, R., Muttiah, R. S. & Williams, J. R. Large area hydrologic modeling and assessment part I: model development. *J. Am. Water Resour. Assoc.* **34**, 73–89 (1998).
50. Gassman, P. W., Sadeghi, A. M. & Srinivasan, R. Applications of the SWAT Model Special Section: Overview and Insights. *J. Environ. Qual.* **43**, 1–8 (2014).
51. Tan, M. L., Gassman, P. W., Yang, X. & Haywood, J. A review of SWAT applications, performance and future needs for simulation of hydro-climatic extremes. *Adv. Water Resour.* **143**, 103662 (2020).
52. Fernandez-Palomino, C. A., Hattermann, F. F., Krysanova, V., Vega-Jácome, F. & Bronstert, A. Towards a more consistent eco-hydrological modelling through multi-objective calibration: a case study in the Andean Vilcanota River basin, Peru. *Hydrol. Sci. J.* **66**, 59–74 (2020).
53. Neitsch, S. L., Arnold, J. G., Kiniry, J. R. & Williams, J. R. Soil & Water Assessment Tool Theoretical Documentation Version 2009. *Texas Water Resour. Institute*, TR-406 1–647 (2011).
54. Fernandez-Palomino, C. A. *et al.* BASD-CMIP6-PE: bias-adjusted and statistically downscaled CMIP6 projections over Peru and Ecuador. *GFZ Data Serv.* <https://doi.org/10.5880/pik.2023.001> (2023).
55. Fiedler, S. *et al.* Simulated Tropical Precipitation Assessed across Three Major Phases of the Coupled Model Intercomparison Project (CMIP). *Mon. Weather Rev.* **148**, 3653–3680 (2020).
56. Almazroui, M. *et al.* Assessment of CMIP6 Performance and Projected Temperature and Precipitation Changes Over South America. *Earth Syst. Environ.* **2021** **5**, 155–183 (2021).
57. Ortega, G., Arias, P. A., Villegas, J. C., Marquet, P. A. & Nobre, P. Present-day and future climate over central and South America according to CMIP5/CMIP6 models. *Int. J. Climatol.* **41**, 6713–6735 (2021).
58. Li, G. & Xie, S. P. Tropical Biases in CMIP5 Multimodel Ensemble: The Excessive Equatorial Pacific Cold Tongue and Double ITCZ Problems. *J. Clim.* **27**, 1765–1780 (2014).
59. Swart, N. C. *et al.* The Canadian Earth System Model version 5 (CanESM5.0.3). *Geosci. Model Dev.* **12**, 4823–4873 (2019).
60. Boucher, O. *et al.* Presentation and Evaluation of the IPSL-CM6A-LR Climate Model. *J. Adv. Model. Earth Syst.* **12**, e2019MS002010 (2020).
61. Sellar, A. A. *et al.* UKESM1: Description and Evaluation of the U.K. Earth System Model. *J. Adv. Model. Earth Syst.* **11**, 4513–4558 (2019).
62. Volodko, A. *et al.* Evaluation of CMIP6 DECK Experiments With CNRM-CM6-1. *J. Adv. Model. Earth Syst.* **11**, 2177–2213 (2019).
63. Séférian, R. *et al.* Evaluation of CNRM Earth System Model, CNRM-ESM2-1: Role of Earth System Processes in Present-Day and Future Climate. *J. Adv. Model. Earth Syst.* **11**, 4182–4227 (2019).
64. Tatebe, H. *et al.* Description and basic evaluation of simulated mean state, internal variability, and climate sensitivity in MIROC6. *Geosci. Model Dev.* **12**, 2727–2765 (2019).

65. Dunne, J. P. *et al.* The GFDL Earth System Model Version 4.1 (GFDL-ESM 4.1): Overall Coupled Model Description and Simulation Characteristics. *J. Adv. Model. Earth Syst.* **12**, e2019MS002015 (2020).
66. Yukimoto, S. *et al.* The Meteorological Research Institute Earth System Model Version 2.0, MRI-ESM2.0: Description and Basic Evaluation of the Physical Component. *J. Meteorol. Soc. Japan. Ser. II* **97**, 931–965 (2019).
67. Müller, W. A. *et al.* A Higher-resolution Version of the Max Planck Institute Earth System Model (MPI-ESM1.2-HR). *J. Adv. Model. Earth Syst.* **10**, 1383–1413 (2018).
68. Döschner, R. *et al.* The EC-Earth3 Earth system model for the Coupled Model Intercomparison Project 6. *Geosci. Model Dev.* **15**, 2973–3020 (2022).
69. Gupta, H. V., Kling, H., Yilmaz, K. K. & Martinez, G. F. Decomposition of the mean squared error and NSE performance criteria: Implications for improving hydrological modelling. *J. Hydrol.* **377**, 80–91 (2009).
70. Kling, H., Fuchs, M. & Paulin, M. Runoff conditions in the upper Danube basin under an ensemble of climate change scenarios. *J. Hydrol.* **424–425**, 264–277 (2012).
71. Gupta, H. V., Sorooshian, S. & Yapo, P. O. Status of Automatic Calibration for Hydrologic Models: Comparison with Multilevel Expert Calibration. *J. Hydrol. Eng.* **4**, 135–143 (1999).
72. Yilmaz, K. K., Gupta, H. V. & Wagener, T. A process-based diagnostic approach to model evaluation: Application to the NWS distributed hydrologic model. *Water Resour. Res.* **44**, (2008).

Acknowledgements

The authors thank the “Brazil East Africa Peru India Climate Capacities (B-EPICC)” project, which is part of the International Climate Initiative (IKI) of the German Federal Ministry for Economic Affairs and Climate Action (BMWK) and is implemented by the Federal Foreign Office (AA). We acknowledge the World Climate Research Programme, which, through its Working Group on Coupled Modelling, coordinated and promoted CMIP6. We thank the climate modeling groups for producing and making available their model output, the Earth System Grid Federation (ESGF) for archiving the data and providing access, and the multiple funding agencies who support CMIP6 and ESGF. We are thankful to Dr. Stefan Lange for making his software “ISIMIP3BASD” available for this study and for providing the unadjusted CMIP6 data. We extend our gratitude to Thomas Nocke for incorporating the BASD-CMIP6-PE dataset into http://www.climateimpactsonline.com/per/index_en.html. This integration facilitates the effective illustration of the potential consequences of climate change on Peru for both users and academia.

Author contributions

C.A.F.P. conceived the study and wrote the first version of the manuscript with inputs from all co-authors, and all authors contributed significantly to further revisions.

Funding

Open Access funding enabled and organized by Projekt DEAL.

Competing interests

The authors declare no competing interests.

Additional information

Correspondence and requests for materials should be addressed to C.A.F.P.

Reprints and permissions information is available at www.nature.com/reprints.

Publisher’s note Springer Nature remains neutral with regard to jurisdictional claims in published maps and institutional affiliations.



Open Access This article is licensed under a Creative Commons Attribution 4.0 International License, which permits use, sharing, adaptation, distribution and reproduction in any medium or format, as long as you give appropriate credit to the original author(s) and the source, provide a link to the Creative Commons licence, and indicate if changes were made. The images or other third party material in this article are included in the article’s Creative Commons licence, unless indicated otherwise in a credit line to the material. If material is not included in the article’s Creative Commons licence and your intended use is not permitted by statutory regulation or exceeds the permitted use, you will need to obtain permission directly from the copyright holder. To view a copy of this licence, visit <http://creativecommons.org/licenses/by/4.0/>.

© The Author(s) 2024